
Volume 49 • Issue 2 • February 2011
ISSN 0008-6223
ELSEVIER
an international journal
Carbon
Reporting research on Carbonaceous Materials, their Production, Properties and Applications
50 nm
Editor-in-Chief: P.A. Thrower
Also available on ScienceDirect www.sciencedirect.com

CARBON 49 (2011) 669–676

available at www.sciencedirect.com

ScienceDirect

journal homepage: www.elsevier.com/locate/carbon

The performance of superhydrophobic and superoleophilic carbon nanotube meshes in water–oil filtration

Chee Huei Lee [a], *Nick Johnson* [b], *Jaroslaw Drelich* [b], *Yoke Khin Yap* [a,*]

[a] *Department of Physics, Michigan Technological University, 1400 Townsend Drive, Houghton, MI 49931, United States*
[b] *Department of Materials Science and Engineering, Michigan Technological University, 1400 Townsend Drive, Houghton, MI 49931, United States*

ARTICLE INFO

Article history:
Received 15 July 2010
Accepted 11 October 2010
Available online 19 October 2010

ABSTRACT

Vertically-aligned multi-walled carbon nanotubes (CNTs) were grown on stainless steel (SS) mesh by thermal chemical vapor deposition with a diffusion barrier of Al_2O_3 film. These three-dimensional porous structures (SS-CNT meshes) were found to be superhydrophobic and superoleophilic. Water advancing contact angles of 145–150° were determined for these SS-CNT meshes in air and oil (gasoline, isooctane). Oil, on the other hand, completely wet the SS-CNT meshes. This combined superhydrophobic and superoleophilic property repelled water while allowed the permeation of oil. Filtration tests demonstrated efficiencies better than 80% of these SS-CNT meshes as the filtration membranes of the water-in-oil emulsions. We have conducted quantitative analysis on the diameters of the oil droplets in both the feed emulsion and the filtrate. Then, we have evaluated the issue of water blockage and possible way to improve the filtration efficiency. Finally, the filtration and blockage mechanisms are proposed.

1. Introduction

Water–oil filtration can be achieved by using the superhydrophobicity and superoleophilicity of porous materials that repel water while allow the permeation of oil, respectively. As inspired by many natural plants, superhydrophobicity also known as the *Lotus effect* [1,2], is generally defined if water contact angle (CA) is larger than 150° and the sliding angle is small, less than 5–10° [3]. Numerous studies have confirmed that combination of microscopic and nanoscopic surface topographies, along with low surface energy material give rise to high water contact angle and low oil contact angle [3–7]. There is a significant research interest to test nanomaterials [8] including carbon nanotubes (CNTs) [9–12], boron nitride nanotubes [13], ZnO [14] and TiO_2 [15] nanowires, as the building blocks of superhydrophobic and oleophilic surfaces. For example, a superhydrophobic surface was created via functionalization of vertically aligned carbon nanotubes with a hydrophobic poly(tetrafluoroethylene) (PTFE) coating [10] or a fluorocarbon film coating [11].

Combining the associated superhydrophobicity and superoleophilicity of nanomaterials, we think that it is possible to construct filters that could separate water from oils and organic solvents. This can be achieved by coating nanomaterials on a supporting mesh. The superhydrophobicity of the nanomaterials will repel water while the associated superoleophilicity allows oil to wet the nanomaterials and pass through such a water–oil filter. However, the durability, and stability of filters for such dewatering applications will depend on the nanomaterials used. Both metals and ceramics are usually preferred over polymeric membranes and cellulose-based filters. Unfortunately, metal and ceramic based filters need intensive modification to improve their hydrophobic and oleophilic properties. For example, nanostructured copper mesh with a variety of treatments such as immersing in NaOH and $K_2S_2O_8$ and subsequent modification with

* *Corresponding author:* Fax: +1 906 487 2933.
E-mail address: ykyap@mtu.edu (Y.K. Ya).
0008-6223/$ - see front matter © 2010 Elsevier Ltd. All rights reserved.
doi:10.1016/j.carbon.2010.10.016

n-dodecanethiol [16], coating the surface with long-chain fatty acids [17], and modification with poly(*N*-isopropylacrylamide) (PNIPAAm) [18] were demonstrated. Stainless steel (SS) mesh coated with a rough surface of PTFE was also reported [19]. Organic and polymeric modifiers, however, are unable to withstand higher temperatures and conduct heat. They are also not very resistant to aggressive liquids such as selected organic solvents, salty, acidic or basic aqueous solutions, common to many industrial emulsions.

CNTs are known as one of the stiffest materials on earth due to their strong sp^2-hybridized carbon tubular networks. The tensile strength of CNTs is 10–20 times higher than that of stainless steel while their Young's modulus is about 5 times higher [20–22]. With their density as low as 1.3–1.4 g/cm^3, the specific strength of carbon nanotubes can reach the value of up to 46 M Nm/kg, more than 300 times higher than for steels [20]. Furthermore, CNTs posses high thermal conductivity (3500 W/mK) [23], and thermal stability between 350–600 °C in air [24,25], making them exceptional for applications at elevated temperatures. In addition, due to their chemical inertness, nanoscale dimensions, and high aspect ratio, CNTs are good candidates for applications in superhydrophobic coatings [9–12] and hydrophobic membranes [16–19]. By combining all these desired properties as well as its superhydrophobic and superoleophilic properties, CNT coating on stainless steel (SS) mesh is applicable for water–oil filtration [26]. Here, quantitative analysis on the diameters of the oil droplets in both the water–oil emulsion and the filtrates is conducted. The filtration mechanism of these CNT meshes is then proposed.

Although many techniques have been used to produce CNTs on various substrates [27–32], chemical vapor deposition (CVD) techniques by either floating ferrocene-derived iron catalyst [33] or thin film type catalyst [10,28], remain the most popular. However, most of these CNTs were grown on flat (2-dimensional) silicon-based substrates. In this article, we report a relatively simple method to directly synthesize vertically aligned multi-walled carbon nanotubes on the rounded rods of a commercially available SS mesh. We show that CNT-coated SS mesh exhibits superhydrophobicity and superoleophilicity, which is applicable for water–oil separation.

2. Experimental procedure

2.1. Growth of CNTs on SS mesh

Thermal CVD technique, as described in details in the previous publication [28], was used to grow CNTs on a 304 SS mesh (325 × 325 mesh). The SS mesh was first cleaned in 12 M HCl for ~10 s and then rinsed with deionized water to remove any possible oxide compound or contamination on the surface. A 35 nm thick Al_2O_3 film was then coated on the SS mesh, followed by a 10 nm thick Fe catalyst film, by pulsed laser deposition (PLD). The catalyst film was pre-treated with H_2 for 10 min at 700 °C in the CVD furnace. It was followed by the CNT growth by introducing 30 sccm (standard cm^3/min) C_2H_2 with 120 sccm H_2 for 10 min. The CNT-coated mesh (SS-CNT) was cooled down to a low temperature in Ar environment for ~1 h before taken out from the furnace.

2.2. Contact angle measurements

Both advancing and receding (static) contact angles (CAs) were measured for water drops placed on the sample surface using a KRUSS-G10 goniometer according to the methodology described previously [13,34]. The advancing and receding CAs are the largest and smallest CA, respectively, measured for the water droplet without increasing its base diameter. The measurements of advancing (receding) CAs were carried out several seconds after small portions of liquid were added (withdrew) to increase (decrease) the volume of the droplet. In this work, 5–8 measurements were carried out for both angles. The average values and standard deviations are reported in this work. During CAs measurements the samples were either surrounded by laboratory air or immersed in oil (isooctane, gasoline 87). All measurements were carried out at room temperature (~22 °C) and the relative humidity of air was 20–30%.

During the measurement, a drop of deionized water, with a diameter of ~2 mm, was formed at the tip of the needle and attached to the sample. The size of the droplet was increased until the base of the drop expanded on the sample surface and the advancing contact angle was measured several seconds after the size of the drop base stopped expansion. After 5–8 measurements of advancing contact angle were completed, the size of the water drop was reduced, until its base contracted, and the receding contact angle was measured. The receding contact angles were measured only for selected systems. Also droplets of isooctane (98%, Aldrich) and gasoline 87 (British Petroleum) were deposited on the SS-CNT mesh. These droplets completely spread over the mesh with near zero contact angles, indicating superoleophilicity of the SS-CNT mesh. As the result, neither advancing nor receding contact angles could be determined for these liquids.

2.3. Emulsion dewatering tests

For the filtration test, the water-in-oil emulsion was prepared by adding 20 mL deionized water to 80 mL of either isooctane or gasoline in a 250 mL flask (ratio = 1:4). In selected tests, a viscous oil (bar & chain oil, distributed by Robert Gruny, Medford, WI), virgin oil lubricant for chain saws was used. The idea of using gasoline and chain oil, beside well-defined organic solvent (isooctane), is to test filtration capability of the SS-CNT mesh on potential contaminated products collected from water or soil after accidental spills. The mixture of liquids was vigorously shaken for 2–3 min. Resulting emulsion was left to settle for 1–2 min before conducting filtration test. The 1–2 min sedimentation time was necessary for the largest water droplets to deposit at the bottom of the flask. A drop of emulsion was spread on a glass slide for microscopic examination. The size and distribution of the water droplets were analyzed under an optical microscope.

A SS-CNT mesh was mounted between two glass tubes having internal diameter of 8 mm and equipped with joints and O-rings. The emulsion was supplied manually to the filtration module using a 5 mL pipette. In total, 20–50 mL of emulsion was passed through the mesh. A flow rate during the filtration test was estimated to be 10–20 mL/(min × cm^2) for isooctane- and gasoline-based emulsions. Effective area of the mesh during filtration was about 0.5 cm^2. Filtrate was collected in a glass beaker and left for sedimentation for several hours to determine amount of water that passed through the mesh with filtrate. A drop of filtrate was also spread over a microscopic glass slide for optical microscopy examination. Microscopic images were analyzed and the number of pixels covered by water droplets was then calculated using a MATLAB program. The ratio of this number versus the total pixel number of the image is taken as the volume concentration of water droplets. This is based on the assumption that the volume concentration of water droplet in the emulsion can be statistically estimated by the 2D area as seen from the microscopic image. On the other hand, the water droplet size distribution was estimated manually by counting the number of droplets at particular size from several microscopic images.

In selected experiments, an electrical current was passed through the SS-CNT mesh in order to investigate the temperature effect on the filtration. In such experiments, only viscous chain oil was used.

3. Results and discussion

3.1. *Properties of the SS-CNT Mesh*

Stainless steel is not a popular substrate for the growth of CNTs as there are not many successful examples [30,35] due to the possible interaction of catalyst with the transitional metals present in the SS composition. At the growth temperature of CNTs, catalyst can easily diffuse into SS to form an alloy. In order to eliminate this situation, a thin layer of

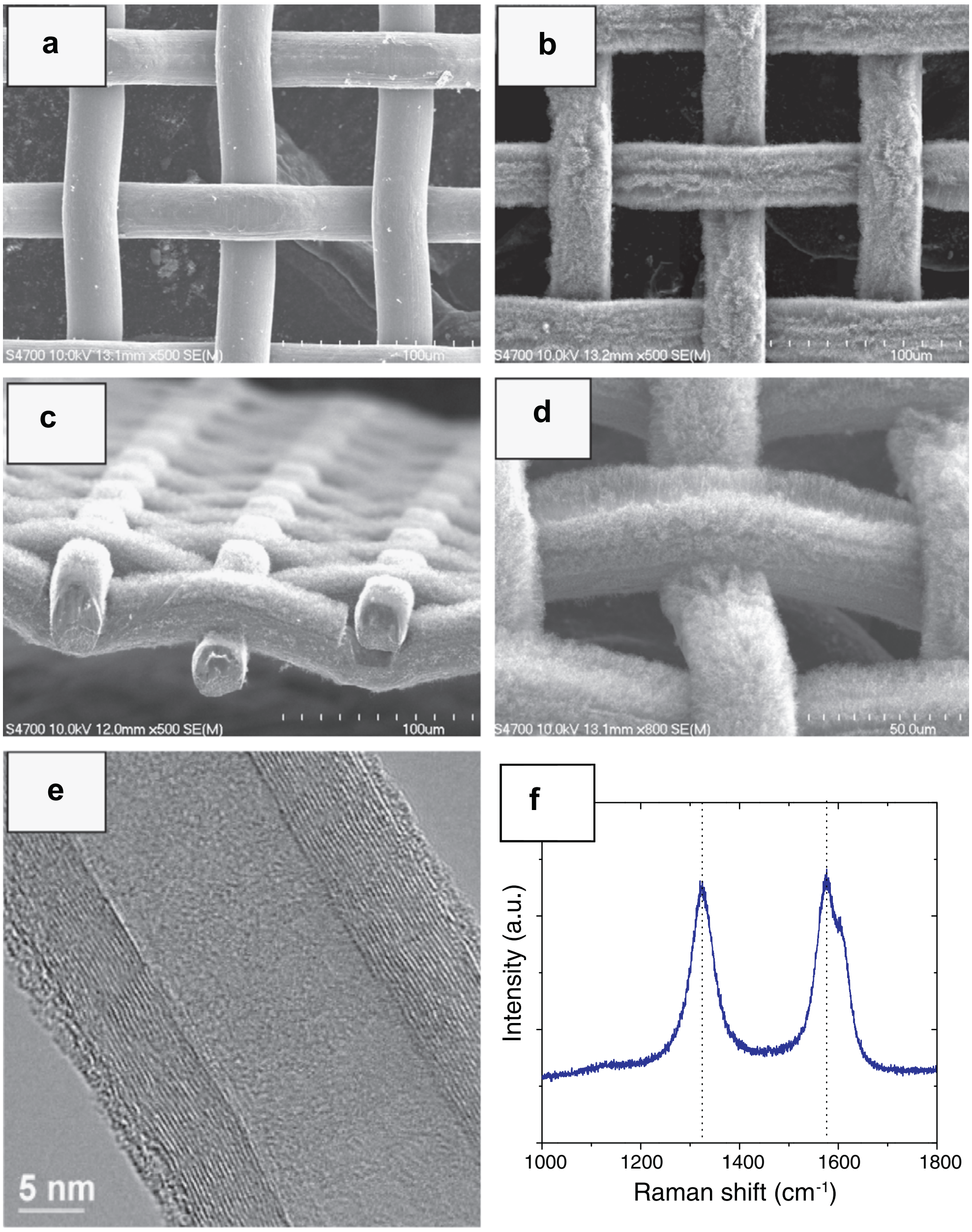

Fig. 1 – SEM images of (a) a bare SS mesh, (b) top view of CNTs grown on a SS mesh, (c and d) a cross sectional view of CNTs grown on a SS mesh, (e) HRTEM image of a CNT, (f) Raman spectrum of the as-grown sample.

Al_2O_3 film was first deposited on the SS mesh as the diffusion barrier. Al_2O_3 diffusion barrier was also shown to be effective for the growth of boron nitride nanotubes at temperatures as high as 1200 °C [36].

Scanning electron microscopy (SEM) images of a bare SS mesh and as-grown CNTs on a SS mesh are shown in Fig. 1a and b for comparison. A forest of vertically-aligned CNTs was deposited on the mesh as shown in the cross sectional views in Fig. 1c and d. The height of the CNT forest is estimated to be >5 μm. Fig. 1e shows the image of high-resolution transmission electron microscopy (HRTEM) for an individual CNT from the mesh. The outer diameter was measured for several CNTs and found to vary typically from ~10 to 30 nm. Raman spectrum (Fig. 1f) reveals D, G and a shoulder of D' carbon peaks at 1325 cm^{-1}, 1578 cm^{-1} and ~1605 cm^{-1} respectively, the characteristic peaks commonly recorded for multi-walled CNTs [37,38].

3.2. Wetting characteristic of SS-CNT mesh

Flat stainless steel surface is poorly wetted by water with advancing water contact angles (CAs) from 55–78°, depending on the surface finish and cleaning [39–42]. On the other hand, the advancing CA for water droplets placed on the bare SS mesh in air was determined to be ~127° (Table 1). This value was much larger than that of a flat surface as the result of openings in between wires. The larger CA on SS mesh is due to the smaller water droplet base area in contact with the mesh wires. This is consistent to the relation described by the Cassie–Baxter (CB) equation: [41] $\cos\theta_{Mesh} = f_a (\cos\theta_{SS} + 1) - 1$, where θ_{Mesh} and θ_{SS} are the contact angles measured on the SS mesh and flat SS surface, respectively, and f_a is the fractional area of the drop base in contact with the mesh wires. Based on the value of θ_{SS} (~67°) and θ_{Mesh} (=127°), f_a was estimated to be ~0.29. However, according to the opening geometry, the f_a value for 325 × 325 mesh is between 0.68 and 0.77, depending whether an area of circular straight wire or a projected area of the wire are taken into calculations. The theoretical value of f_a is much lower than that of the geometrical analysis, suggesting that the overlapping and bending wires in the mesh (Fig. 1a and c) reduce the actual contact area between water and SS mesh. In fact, the CB equation applies to equilibrium contact angles. Since equilibrium contact angles are impossible or difficult to measure for structured substrates, advancing contact angles are often used instead. Advancing contact angles more closely represent wetting characteristic of materials than receding contact angles, which are more sensitive to structural and chemical imperfections of the substrates.

Vertically-aligned CNTs produced a superior enhancement of the hydrophobicity of the SS mesh. The advancing water CA on the SS-CNT mesh was measured to be ~150° (Table 1). Carbon-based products such as graphite and graphene are more hydrophobic than SS with water CA from 82–86° [43]. For CNTs, water CAs as high as 150–170° were reported [10,12]. Based on the CB equation, $\cos\theta_{SS\text{-}CNT} = f_{CNT} (\cos\theta_C + 1) - 1$, where $\theta_{SS\text{-}CNT}$ (=150°) and θ_C (=82–86°) are the contact angles measured on the SS-CNT mesh and carbon material (graphite). The f_{CNT} is estimated to be ~0.12. This value indicates, as expected, that a water droplet has smaller contact area with SS-CNT mesh than with SS mesh (as estimated earlier, $f_a = 0.29$). Hydrophobicity and small diameters of CNTs prevent water from penetration into less hydrophobic SS mesh.

As shown in Table 1, suspension of water droplets in oil instead of air did not significantly affect the CAs on both bare SS mesh and SS-CNT mesh. We observed that water droplets rolled off from the mesh surface easily in air or oil, indicating on a very small sliding angle. The receding water CAs were only a few degrees smaller than advancing water CAs (Table 1). As a comparison, the receding CAs on a SS mesh without CNTs were always near zero value. Besides, a water droplet always pined on the bare SS mesh even it was put upside down. These observations and measurements confirmed high CA hysteresis for a bare SS mesh.

In addition, we found that droplets of isooctane and gasoline spread on the SS-CNT mesh and drained through the mesh. This means the SS-CNT mesh is superoleophilic. Although neither advancing nor receding contact angles could be measured precisely for these liquids, the contact angles zero or nearly zero value could be deduced from microscopic observations and are results of superoleophilic nature of the porous SS-CNT mesh.

3.3. Water–oil filtration

After confirming the superhydrophobicity and superoleophilicity of our SS-CNT mesh, we then proceeded to the water–oil filtration experiments. First, we found that water droplets with the diameter of 3–7 mm can reside on the SS-CNT mesh over a period of several hours, showing no sign of water penetration through the mesh. This means, our SS-CNT mesh maintain a stable superhydrophobicity.

Fig. 2 shows examples of water droplets suspended on the SS-CNT mesh in air and immersed in isooctance. Similar results were observed for gasoline with water (not shown). Several water-in-oil emulsion filtration tests were then performed using the SS-CNT mesh. Gasoline was used as a

Table 1 – Advancing and receding contact angles (CAs) measured for water droplets on SS mesh and SS-CNT mesh in different fluids (ND = not determined).

SS-CNT Mesh			Bare SS mesh		
Surrounding fluid	Water CA [deg] Advancing [deg]	Receding [deg]	Surrounding fluid	Water CA [deg] Advancing [deg]	Receding [deg]
Air	150 ± 3	143 ± 6	Air	127 ± 5	<10
Isooctane	147 ± 9	142 ± 5	Isooctane	133 ± 2	10–15
Gasoline 87	145 ± 4	ND	Gasoline 87	129 ± 4	ND

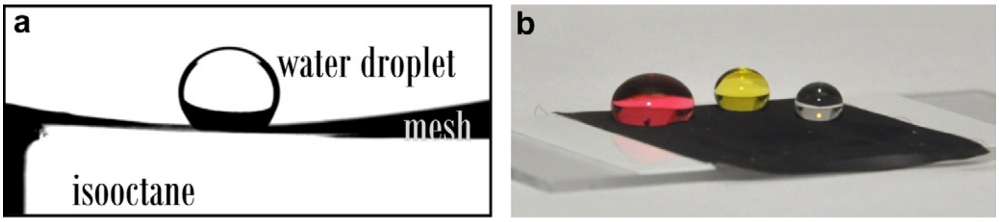

Fig. 2 – Water droplets suspended on SS-CNT mesh in (a) isooctance, and (b) air. Water of different pH was colored with methyl red.

continuous phase in the tests and water was dispersed in it at a concentration from about 5–10 wt.%. Emulsions prepared for a filtration test were opaque due to dispersed water. Diameter of water droplets dispersed varied mostly from about 3 to over 100 μm. Fig. 3 shows optical microscopy images for one of the samples tested, together with droplet size distribution diagram.

In a typical test, 20–50 mL of emulsion was effectively filtrated through the SS-CNT mesh. In selected experiments, 3.0–3.2 A current and 1.4–1.6 V were applied to the SS-CNT mesh, which resulted in a raise of the mesh temperature to 120–150 °C in seconds. In such experiments viscous chain oil was used instead of gasoline. The heating of the mesh did enhance the kinetics of filtration, increasing at least 2–3 times the flow rate of viscous emulsion passing through the mesh. However, the efficiency of dewatering was not significantly improved.

After the filtration through the SS-CNT mesh, the amount of water in the gasoline was significantly reduced. It was observed that the efficiency of dewatering was influenced by the water droplet size distribution in the feed emulsion, duration of filtration, and height of emulsion column placed on the mesh during filtration. Most of the experiments were carried out using emulsion with the water content of above 7 wt.%,

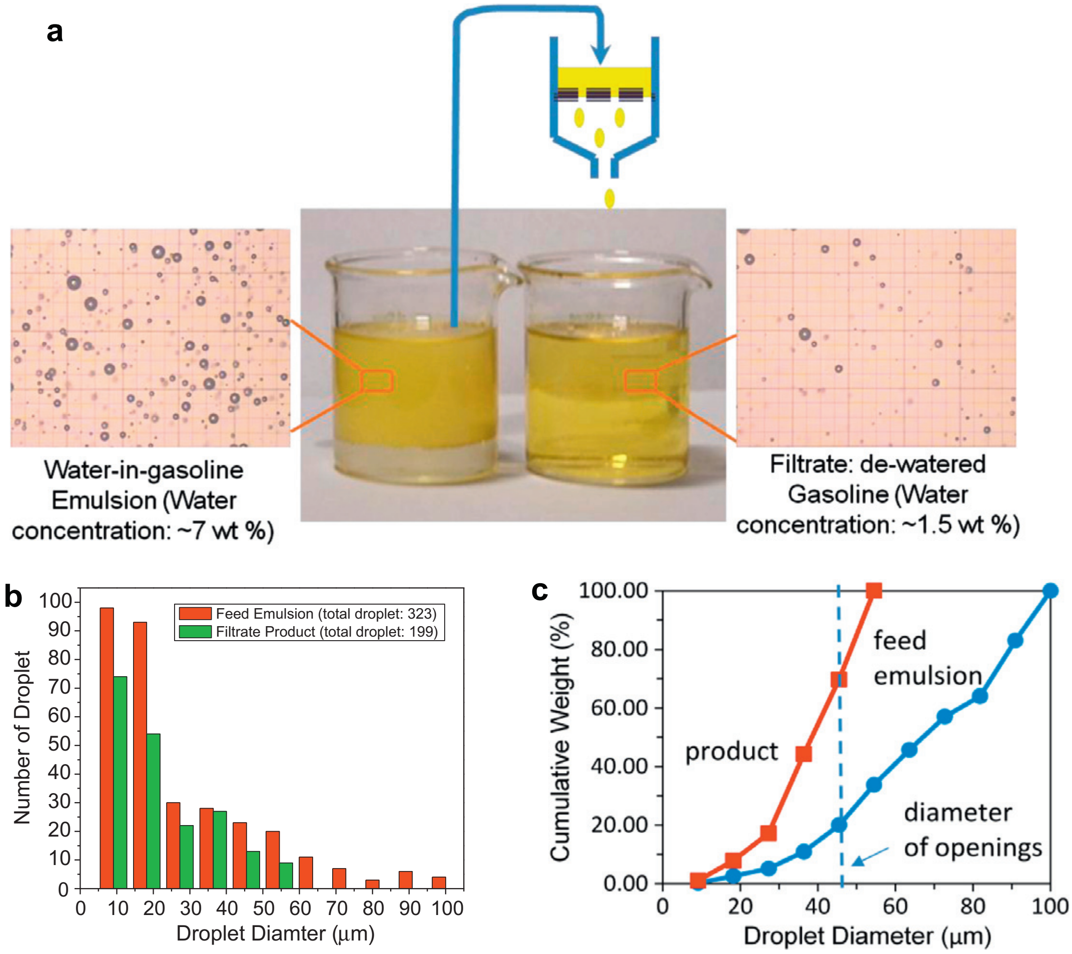

Fig. 3 – (a) Photographs of beakers with the water-in-oil feed emulsion and filtrate obtained during the filtration test. (b) Histogram of the size distribution of water droplet. (c) Cumulative water droplet size distribution curves for the feed emulsion and the product (filtrate).

which was then reduced to less than 1.5 wt.% in the filtrate, preventing ~80 wt.% of water to pass through the mesh as described hereafter. As shown by the images in Fig. 3a, the filtrate contained smaller population of the water droplets. Quantitative analysis of water droplet size distribution confirmed that the majority of the droplets in both the feed emulsion and the product (filtrate) are smaller than the size of the mesh openings (~45 μm) (Fig. 3b).

The corresponding cumulative weight versus the water droplet diameter is presented in Fig. 3c. To calculate the cumulative weight, the respective weight percentage (wt.%) was first calculated using the following formula: $\text{wt.\%} = \frac{n_i \rho V_i}{\sum_{i=1} n_i \rho V_i} 100\%$, where n_i is the number of the water droplets in certain diameter range i, ρ is the density of water, and V_i is the average volume of the droplet in the diameter range i. The cumulative weight is the weight percentage at particular diameter range plus the sum of the weight percentages for droplets with smaller diameters. The blue curve in Fig. 3c shows that the feed emulsion contained only ~20 wt.% of water as droplets with diameter <45 μm although the number of such droplets are high as shown in Fig. 3b. Eighty wt.% of water droplets in the feed emulsion have diameter larger than the size of mesh openings (>45 μm), which will not pass through the SS-CNT mesh. On the other hand, majority of water droplets (~70 wt.%) in the product (red curve) had diameter smaller than openings in the mesh (<45 μm), confirming that the mesh was unable to prevent the pass of fine droplets.

Nevertheless, we also found that some water was trapped on the SS-CNT mesh, blocking individual openings of the mesh. Fig. 4 shows the image of the SS-CNT mesh taken immediately after filtration test. A significant portion of the effective area of the mesh was covered with water droplets that were approximately the size of individual segments of the mesh (Fig. 4). We also observed that partial removal of water droplets smaller than the size of mesh openings could occur, especially at the beginning of filtration and when low flow rates were used. It is speculated that water droplets repelled by CNTs may prompt to a coalescence process as schematically shown in Fig. 5. However, enlarged water droplets finally could cover individual openings of the mesh, reducing the effective area for filtration as was reflected in a reduced

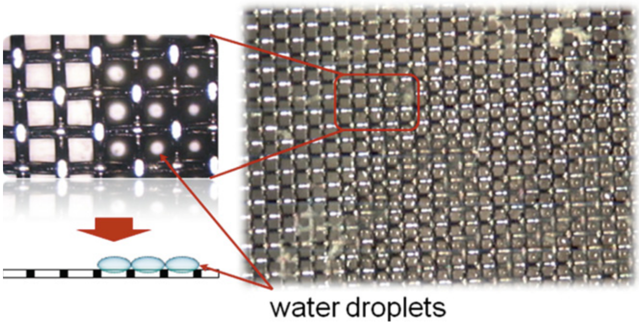

Fig. 4 – Optical microscopy images of the mesh used in filtration test. Many openings of the mesh were covered with microscopic size water droplets after filtration suggesting entrapment and/or growth of water droplets in openings during filtration. Possible mechanisms of formation of such water "gates" are shown in Fig. 5.

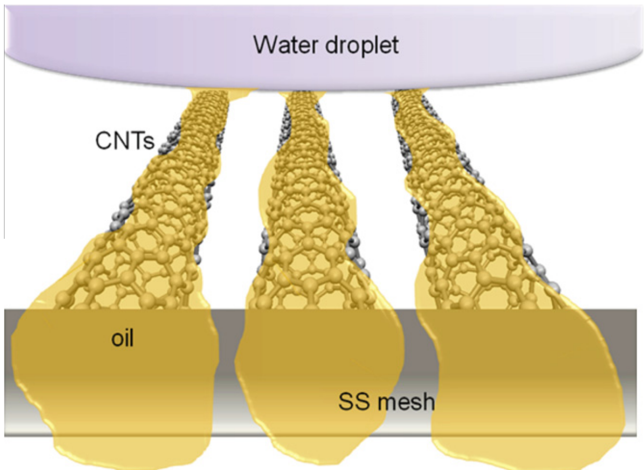

Fig. 6 – The associated hydrophobicity and oleophilicity of CNTs on the SS-CNT mesh.

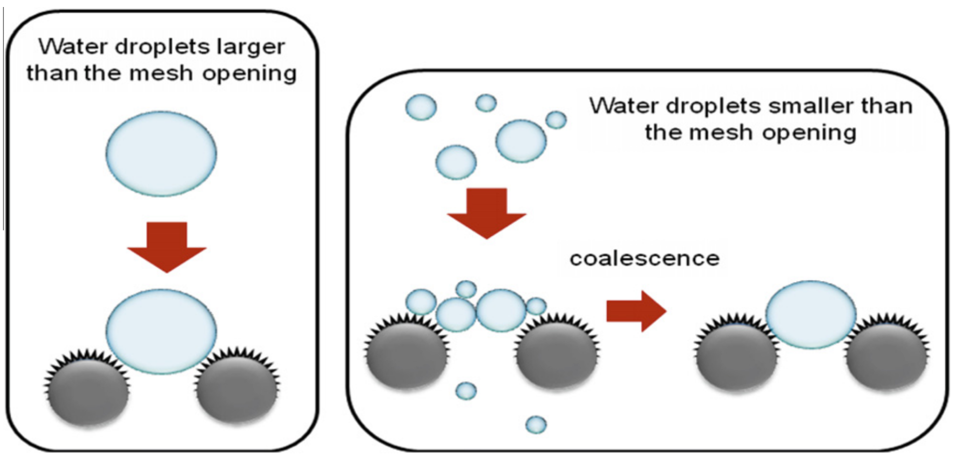

Fig. 5 – Illustration of possible mechanisms during the filtration of water-in-oil emulsion that led to entrapment and formation of microscopic water droplets in mesh openings.

liquid flow rate observed in our tests. We think that water that accumulated on the mesh could pass through the SS-CNT mesh under hydraulic pressure and reducing the filtration efficiency. The use of cross-flow filtration scheme that would continuously remove water away from the filter could probably eliminate this problem.

Finally, the associated superhydrophobicity and superoleophilicity of CNTs on our SS-CNT mesh can be schematically illustrated in Fig. 6. This is a bottom-up view, looking upward from the SS-CNT mesh to the water-in-oil emulsion on top of the CNT tips. As shown, a water droplet (top sphere) is in contact with the tips of CNTs. Since CNTs are hydrophobic, water is prevented from wetting the side walls of CNTs. On the other hand, due to the oleophilicity of CNTs, oil surrounding the water droplet will wet the side walls of CNTs and propagate downward to the filter due to gravitation force. This will allow the flow of oil on the side walls of CNTs and finally pass through the SS mesh underneath as the filtrate.

4. Conclusion

We demonstrated a simple procedure to grow vertically-aligned CNTs on 3-dimensional and flexible stainless steel mesh by thermal chemical vapor deposition technique. The as-fabricated SS-CNT mesh has the ability to dewater water–oil emulsion. Based on our quantitative analysis on the diameters of the oil droplets in both the feed emulsion and the filtrate, we think that the filtration efficiency depends on the initial droplet sizes of the oil in the feed emulsion. Water blockage issues and the related mechanisms are discussed. We propose that successful use of CNTs in such water–oil filtration is due to the fact that CNTs have higher affinity to oil than to water due to the hydrophobic interaction between oil molecules and the graphene sheets of CNTs.

Acknowledgement

Yoke Khin Yap acknowledges supports from the National Science Foundation *CAREER* award (award number 0447555). Nick Johnson appreciates the McArthur Research Internship that supported his contribution to the research program described in this paper.

REFERENCES

[1] Barthlott W, Neinhuis C. Purity of the sacred lotus, or escape from contamination in biological surfaces. Planta 1997;202(1):1–8.

[2] Neinhuis C, Barthlott W. Characterization and distribution of water-repellent, self-cleaning plant surfaces. Ann Bot 1997;79(6):667–77.

[3] Sun T, Feng L, Gao X, Jiang L. Bioinspired surfaces with special wettability. Acc Chem Res 2005;38(8):644–52.

[4] Roach P, Shirtcliffe NJ, Newton MI. Progress in superhydrophobic surface development. Soft Matter 2008;4:224–40.

[5] Kim SH. Fabrication of superhydrophobic surfaces. J Adhes Sci Technol 2008;22:235–50.

[6] Miller JD, Veeramasuneni S, Drelich J, Yalamanchili MR, Yamauchi G. Effect of roughness as determined by atomic force microscopy on the wetting properties of PTFE thin films. Polym Eng Sci 1996;36(14):1849–55.

[7] Veeramasuneni S, Drelich J, Miller JD, Yamauchi G. Hydrophobicity of ion-plated PTFE coatings. Prog Org Coat 1997;31(3):265–70.

[8] Ma M, Hill RM, Rutledge GC. A review of recent results on superhydrophobic materials based on micro- and nanofibers. J Adhes Sci Technol 2008;22:1799–817.

[9] Georgakilas V, Bourlinos AB, Zboril R, Trapalis C. Synthesis, characterization and aspects of superhydrophobic functionalized carbon nanotubes. Chem Mater 2008;20(9):2884–6.

[10] Lau KKS, Bico J, Teo KBK, Chhowalla M, Amaratunga GAJ, Milne WI, et al. Superhydrophobic carbon nanotube forests. Nano Lett 2003;3(12):1701–5.

[11] Zhu L, Xiu Y, Xu J, Tamirisa PA, Hess DW, Wong C-P. Superhydrophobicity on two-tier rough surfaces fabricated by controlled growth of aligned carbon nanotube arrays coated with fluorocarbon. Langmuir 2005;21(24):11208–12.

[12] Sethi S, Ge L, Ci L, Ajayan PM, Dhinojwala A. Gecko-inspired carbon nanotube-based self-cleaning adhesives. Nano Lett 2008;8(3):822–5.

[13] Lee CH, Drelich J, Yap YK. Superhydrophobicity of boron nitride nanotubes grown on silicon substrates. Langmuir 2009;25(9):4853–60.

[14] Feng X, Feng L, Jin M, Zhai J, Jiang L, Zhu D. Reversible super-hydrophobicity to super-hydrophilicity transition of aligned ZnO nanorod films. J Am Chem Soc 2004;126(1):62–3.

[15] Lai Y, Lin C, Wang H, Huang J, Zhuang H, Sun L. Superhydrophilic–superhydrophobic micropattern on TiO_2 nanotube films by photocatalytic lithography. Electrochem Commun 2008;10(3):387–91.

[16] Pan Q, Wang M, Wang H. Separating small amount of water and hydrophobic solvents by novel superhydrophobic copper meshes. Appl Surf Sci 2008;254(18):6002–6.

[17] Wang S, Song Y, Jiang L. Microscale and nanoscale hierarchical structured mesh films with superhydrophobic and superoleophilic properties induced by long-chain fatty acids. Nanotechnology 2007;18(1):015103.

[18] Song W, Xia F, Bai Y, Liu F, Sun T, Jiang L. Controllable water permeation on a poly(N-isopropylacrylamide)-modified nanostructured copper mesh film. Langmuir 2006;23(1):327–31.

[19] Feng L, Zhang Z, Mai Z, Ma Y, Liu B, Jiang L, et al. A super-hydrophobic and super-oleophilic coating mesh film for the separation of oil and water13. Angew Chem Int Ed 2004;43(15):2012–4.

[20] Yu M-F, Lourie O, Dyer MJ, Moloni K, Kelly TF, Ruoff RS. Strength and breaking mechanism of multiwalled carbon nanotubes under tensile load. Science 2000;287(5453):637–40.

[21] Demczyk BG, Wang YM, Cumings J, Hetman M, Han W, Zettl A, et al. Direct mechanical measurement of the tensile strength and elastic modulus of multiwalled carbon nanotubes. Mater Sci Eng., A 2002;334(1–2):173–8.

[22] Sinnott SB, Andrews R. Carbon nanotubes: synthesis, properties, and applications. Crit Rev Solid State Mater Sci 2001;26(3):145–249.

[23] Pop E, Mann D, Wang Q, Goodson K, Dai H. Thermal conductance of an individual single-wall carbon nanotube above room temperature. Nano Lett 2005;6(1):96–100.

[24] Arepalli S, Nikolaev P, Gorelik O, Hadjiev VG, Holmes W, Files B, et al. Protocol for the characterization of single-wall carbon nanotube material quality. Carbon 2004;42(8–9):1783–91.

[25] Itkis ME, Perea DE, Jung R, Niyogi S, Haddon RC. Comparison of analytical techniques for purity evaluation of single-

walled carbon nanotubes. J Am Chem Soc 2005;127(10):3439–48.
[26] Lee C, Baik S. Vertically-aligned carbon nano-tube membrane filters with superhydrophobicity and superoleophilicity. Carbon 2010;48(8):2192–7.
[27] Hiraoka T, Yamada T, Hata K, Futaba DN, Kurachi H, Uemura S, et al. Synthesis of single- and double-walled carbon nanotube forests on conducting metal foils. J Am Chem Soc 2006;128(41):13338–9.
[28] Kayastha VK, Wu S, Moscatello J, Yap YK. Synthesis of vertically aligned single- and double-walled carbon nanotubes without etching agents. J Phys Chem C 2007;111(28):10158–61.
[29] Holt JK, Park HG, Wang Y, Stadermann M, Artyukhin AB, Grigoropoulos CP, et al. Fast mass transport through sub-2-nanometer carbon nanotubes. Science 2006;312(5776):1034–7.
[30] Sethi S, Dhinojwala A. Superhydrophobic conductive carbon nanotube coatings for steel. Langmuir 2009;25(8):4311–3.
[31] Hata K, Futaba DN, Mizuno K, Namai T, Yumura M, Iijima S. Water-assisted highly efficient synthesis of impurity-free single-walled carbon nanotubes. Science 2004;306(5700):1362–4.
[32] Talapatra S, Kar S, Pal SK, Vajtai R, Ci L, Victor P, et al. Direct growth of aligned carbon nanotubes on bulk metals. Nat Nano 2006;1(2):112–6.
[33] Srivastava A, Srivastava ON, Talapatra S, Vajtai R, Ajayan PM. Carbon nanotube filters. Nat Mater 2004;3(9):610–4.
[34] Drelich J, Miller JD, Good RJ. The effect of drop (Bubble) size on advancing and receding contact angles for heterogeneous and rough solid surfaces as observed with sessile-drop and captive-bubble techniques. J Colloid Interface Sci 1996;179(1):37–50.
[35] Baddour CE, Fadlallah F, Nasuhoglu D, Mitra R, Vandsburger L, Meunier J-L. A simple thermal CVD method for carbon nanotube synthesis on stainless steel 304 without the addition of an external catalyst. Carbon 2009;47(1):313–8.
[36] Lee CH, Xie M, Kayastha V, Wang J, Yap YK. Patterned growth of boron nitride nanotubes by catalytic chemical vapor deposition. Chem Mater 2010;22(5):1782–7.
[37] Kayastha VK, Yap YK, Pan Z, Ivanov IN, Puretzky AA, Geohegan DB. High-density vertically aligned multiwalled carbon nanotubes with tubular structures. Appl Phys Lett 2005;86(25):253105.
[38] Antunes EF, Lobo AO, Corat EJ, Trava-Airoldi VJ, Martin AA, Veríssimo C. Comparative study of first- and second-order Raman spectra of MWCNT at visible and infrared laser excitation. Carbon 2006;44(11):2202–11.
[39] Roero C. Contact-angle measurements of sessile drops deformed by a DC electric field. In: Mittal KL, editor. Contact Angle, Wettability and Adhesion, Vol. 4. Leiden, The Netherlands VSP 2006. p. 165–76.
[40] Bren L, English L, Fogarty J, Policoro R, Zsidi A, Vance J, et al. Hydrophilic/electron-acceptor surface properties of metallic biomaterials and their effect on osteoblast cell activity. J Adhes Sci Technol 2004;18(15–16):1711–22.
[41] Cassie ABD, Baxter S. Wettability of porous surfaces. Trans Faraday Soc 1944;40:546–51.
[42] Mantel M, Wightman JP. Influence of the surface chemistry on the wettability of stainless steel. Surf Interface Anal 1994;21(9):595–605.
[43] Adamson AW, Gast AP. Physical Chemistry of Surfaces. 6th ed. New York: John Wiley & Sons, Inc.; 1997. p. 365.